Ultrasound in Med. & Biol., Vol. ■■, No. ■■, pp. ■■–■■, 2018

0301-5629/$ - see front matter

https://doi.org/10.1016/j.ultrasmedbio.2018.03.004

● *Original Contribution*

HIGH-DYNAMIC-RANGE ULTRASOUND: APPLICATION FOR IMAGING TENDON PATHOLOGY

Yiming Xiao,*,† Mathieu Boily,‡ Hoda Sadat Hashemi,† and Hassan Rivaz*,†

* PERFORM Centre, Concordia University, Montreal, Quebec, Canada; † Department of Electrical and Computer Engineering, Concordia University, Montreal, Quebec, Canada; and ‡ Department of Diagnostic Radiology, McGill University, Montreal, Quebec, Canada

(*Received* 13 *November* 2017; *revised* 25 *February* 2018; *in final form* 2 *March* 2018)

Abstract—Raw ultrasound (US) signal has a very high dynamic range (HDR) and, as such, is compressed in B-mode US using a logarithmic function to fit within the dynamic range of digital displays. However, in some cases, hyperechogenic tissue can be overexposed at high gain levels with the loss of hypo-echogenic detail at low gain levels. This can cause the loss of anatomic detail and tissue texture and frequent and inconvenient gain adjustments, potentially affecting the diagnosis. To mitigate these drawbacks, we employed tone mapping operators (TMOs) in HDR photography to create HDR US. We compared HDR US produced from three different popular TMOs (Reinhard, Drago and Durand) against conventional US using a simulated US phantom and *in vivo* images of patellar tendon pathologies. Based on visual inspection and assessments of structural fidelity, image entropy and contrast-to-noise ratio metrics, Reinhard and Drago TMOs substantially improved image detail and texture. (E-mail: yiming.xiao@concordia.ca)

Key Words: **Ultrasound, High dynamic range, Tone mapping, Tendon pathology, Image processing.**

INTRODUCTION

As a cost-effective and accessible imaging modality, ultrasound (US) allows physicians to obtain diagnostic images in real time. Before US images can be displayed on the monitor, a logarithmic function is used to compress the image intensities to fit within the restrictive dynamic range of the digital display because usually the original signal has a much higher dynamic range. However, with this simple dynamic range compression technique, it can be difficult to clearly display body regions that contain tissues with a wide range of echogenicity, such as at the presence of bones or metals in one image. In other words, either hyper-echogenic regions of the image become overexposed (too bright) or hypo-echogenic regions become underexposed (too dark). This has three major impacts. First, it can lead to the loss of anatomic detail and tissue texture that may be instrumental for diagnosis, especially considering US images are often archived as snapshots of the display in the clinic. Second, gain adjustment is time consuming and can further lead to inter- and intra-physician inconsistency for the same and across different clinical cases. Previous studies (Peters et al. 2013; Potter et al. 2008) revealed that variability in gain settings can greatly affect clinical evaluations. Furthermore, such inconsistency may hinder the potential of US as a modality in longitudinal study of diseases. Lastly, as gain adjustment is typically performed multiple times during the same session and between sessions, it can be inconvenient for certain examinations that require switching the operating hand between the control panel and the scanning region. To facilitate US examinations, there is an extensive literature (Perperidis 2016) on techniques to improve image contrast. Some have proposed improving image quality through spatial and frequency compounding (Cincotti et al. 2001); others employed speckle removal (Achim et al. 2001) or tissue harmonic imaging to enhance scan contrast (Shapiro et al. 1998). Other groups also aimed to automatically optimize the image dynamic range or gain control to minimize unnecessary user interaction with the scanner. More specifically, Lee et al. (2015) proposed adaptively adjusting the dynamic range value by manipulating input images similar to a reference image. With respect to gain adjustment, another group (Lee et al. 2006)

Address correspondence to: Yiming Xiao, PERFORM Centre, Concordia University, 7200 Sherbrooke Street West, Room 2.211, Montreal, Quebec H4B 1R6, Canada. E-mail: yiming.xiao@concordia.ca

suggested optimizing the time gain compensation (TGC) by assuming that log-compressed echo signals attenuate uniformly along the depth. Integrating various metrics and estimates of ultrasound physical and imaging properties, Moshavegh et al. (2015) performed automated gain adjustments to address the drastic attenuation variations between different media. Unfortunately, to date, the aforementioned issues stemming from the restrictive dynamic range of B-mode US display are still not resolved, and a new technique is needed.

For optical cameras, on the one hand, a long exposure helps in photographing objects in the dark, but at the cost of saturating image detail in the well-lit regions. On the other hand, a short exposure is required for photographing fine detail in the bright light. To improve image detail under uneven lighting conditions of the same scene, high-dynamic-range (HDR) photography combines photographs taken under multiple exposures into a single picture with extended dynamic range. To properly display the photo, a tone mapping operator (TMO) is typically used to adapt the HDR image into a smaller dynamic range. These image processing techniques are now commonly used in mobile phones and computers to improve the quality of photographs. HDR techniques are highly pertinent in US imaging given the high dynamic range of the raw radiofrequency (RF) signal.

In this study, we proposed employing tone mapping on the Hilbert-transformed RF data to improve the visualization of image features with a wide range of echogenicity at the convenience of no 2-D manual gain adjustments for the conventional log-compression technique. We compared three different popular tone mapping techniques (Drago et al. 2003; Durand and Dorsey 2002; Reinhard and Devlin 2005) first on a simulated US phantom image and then for the application of imaging patellar tendon pathologies, because the tendon images typically contain various tissue types, including bones, muscles, tendons and potentially liquids, and such a large range of echogenicity requires appropriate gain adjustments to properly display the image content. HDR ultrasound is expected to facilitate diagnostic procedures in the clinic.

METHODS

Tone mapping operators

Many tone mapping techniques have been introduced in the past (Eilertsen et al. 2017), which can generally be classified as global and local types. A global TMO applies the same intensity mapping function over the entire image. In contrast, a local operator applies the mapping function that varies spatially depending on the image characteristics of the target pixel's neighborhood. Although the global operators tend to be more computationally efficient, the local operator can better bring up local image contrast. For the work described here, we used three popular tone mapping operators for the application of imaging patellar tendon pathologies, including the TMOs of Reinhard and Devlin (2005), Drago et al. (2003) and Durand and Dorsey (2002). Although the first two are global TMOs, the last is a local TMO. Inspired by photoreceptor physiology, Reinhard and Devlin (2005) used sigmoid functions that modeled the retinal response of cones and rods for the luminance compression. Based on logarithmic compression of luminance values, imitating the human response to light, the technique of Drago et al. (2003) intends to compress image intensity by adaptively varying the logarithmic bases depending on the local luminance. To do so, a bias power function is introduced to dynamically determine the logarithmic bases, resulting in good preservation of detail and contrast. Lastly, the TMO of Durand and Dorsey uses an edge-preserving bilateral filter (Tomasi and Manduchi 1998) to decompose the original image into a base layer and a detail layer. The contrast of the base layer, which has low-spatial-frequency contents, is reduced and recombined with the detail layer that preserves the high-frequency structural detail. The technique is fast and addresses the halo artifacts (objects appear glowing in the image) and diffusion at discontinuities in some earlier local tone mapping methods.

Phantom US simulation

To assess the performance of different dynamic range reduction techniques, we first simulated an ultrasound image of a tissue-mimicking phantom using the Field II software package (Jensen 1996). The phantom is a cube $36 \times 40 \times 10$ mm (height × width × thickness); 1.2×10^5 scatterers with Gaussian scattering strengths are distributed uniformly in the phantom. Six spherical lesions with radii of 3 mm and three point scatterers were placed inside the phantom. As illustrated in Figure 1, region 1 is a cyst lesion (no scatterers), and the amplitudes of regions 2–6 are that of the background multiplied by factors of 2, 5, 10, 100 and 1000, respectively. The focus of the US beams was placed at the depth of the second point scatterer. Hilbert transformation was applied to the simulated RF signal, and different tone mapping operators mentioned earlier and the log-compression method were used on the amplitude modulated image. Finally, the image intensities were linearly scaled to the range [0,255] to fit the dynamic range of a typical digital display. As seen in Figure 1, with log compression, the contrast of the lesions with lower amplitudes disappears as the gain decreases, and in the uncompressed images, only the lesion with the most hyper-intensive signals can be seen. It will be explained in the Results that this issue is resolved using the proposed HDR techniques.

Patient data acquisition

The Ministère de la Santé et des Services Sociaux provided ethical approval to collect data from human

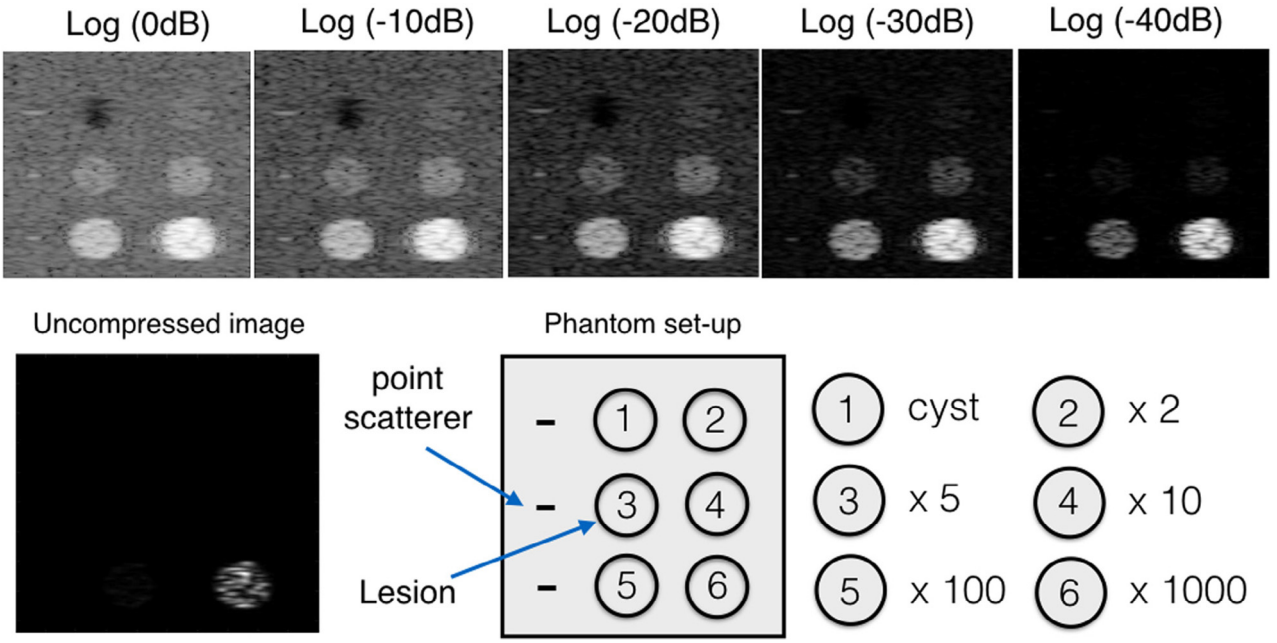

Fig. 1. Simulated US data of a phantom. Top row: Log-compressed scans of the phantom at different gains. Bottom left: Image before compression. Bottom right: Construction of the phantom.

patients at Concordia University's PERFORM Centre. Eight university athletes between the ages of 18 and 25 y who had symptomatic patellar tendons were recruited. They had recently been diagnosed in the clinic and undergone on-site ultrasound inspection and MRI scans of their injured knees. All of these patients suffered from mild or moderate tendinosis in one or both of their patellar tendons, and intra-substance tears were observed in four patients. On receipt of informed consent, ultrasound scans of their injured patellar tendons were obtained by an experienced fellowship-trained musculoskeletal radiologist (M.B.) using the E-cube R12 scanner (Alpinion, Bothell, WA, USA) with an L3-12 linear transducer at the center frequency of 11 MHz and sampling frequency of 40 MHz, and the raw beam-formed RF signals (16 bits) were saved. For each injured knee, longitudinal ultrasound of the patellar tendon was obtained, and two US frames acquired at two adjacent positions by moving the transducer slightly in the transverse direction were used for our experiments. Thus, 22 sets of RF signals in total were saved. The pathologies seen in US images were confirmed and manually contoured by the same radiologist (M.B.). Amplitude demodulation was performed using Hilbert transformation of the beam-formed RF signal, and then the results were processed with HDR tone mapping operators mentioned earlier, as well as the traditional log-compression method. All resulting images were linearly scaled to the range [0,255] to fit the dynamic range of the digital display.

Evaluation metrics

Three metrics were used to evaluate the reproduction of image detail from the original HDR data and the richness of image detail, as well as image quality for inspecting pathologies. The raw US signals contain rich image detail with an extended intensity range. To evaluate the quality of replicating this detail through tone mapping, we employed the structural fidelity metric (Yeganeh and Wang 2013) to compare the raw HDR image and tone mapped images. The local structural fidelity is defined as

$$SF_{local} = \frac{2\sigma'_x\sigma'_y + C_1}{\sigma'^2_x + \sigma'^2_y + C_1} \cdot \frac{\sigma_{xy} + C_2}{\sigma_x\sigma_y + C_2} \tag{1}$$

where σ_x, σ_y and σ_{xy} are the local deviations and cross-correlation between two corresponding patches x and y from the image without intensity compression and the low-dynamic-range (LDR) image, respectively, $C_1 = 0.01$, and $C_2 = 10$. Here, σ'_x and σ'_y are obtained by passing σ_x and σ_y through a non-linear mapping function to penalize cases where contrast is significant in one patch but not in the other. Here, a patch size of 9×9 pixels was used, and the non-linear mapping function is defined as

$$\sigma' = \begin{cases} 0, & \sigma < T_1 \\ \frac{1}{2}\left\{1 + cos\left[\frac{\pi}{T_2 - T_1}(\sigma - T_2)\right]\right\}, & T_1 \le \sigma \le T_2 \\ 1, & T_2 < \sigma, \end{cases} \tag{2}$$

where $T_1 = 0.5$ and $T_2 = 4$. The final structural fidelity is the average of all local measurements over the entire image, with a range of [0,1] and 0 being the worst quality of tone mapping.

With improved tone mapping, subtle structural details can be better delineated. To assess the improvement in the richness of image detail, we used image entropy:

$$Entropy = -\sum_i p_i log(p_i) \quad (3)$$

where p_i is the normalized image intensity histogram counts of the ith bin. In total, 256 bins were used. A higher entropy value represents richer detail in an image.

Lastly, in addition to the overall appearance of the image, we also measured the contrast-to-noise ratios (CNRs) of relevant image features. Relevant regions of interest (ROIs) were used to compute the CNR, which is defined as

$$CNR = \sqrt{\frac{2(S_A - S_B)^2}{\sigma_A^2 + \sigma_B^2}} \quad (4)$$

where S_A and S_B are the spatial means of the image in regions A and B, and σ_A^2 and σ_B^2 are the variances of regions A and B, respectively. A higher CNR means better visual contrast between adjacent regions A and B. For the simulated phantom, CNRs of the lesions were measured against the background. For the *in vivo* tendon data, we evaluated the CNRs between the tendinosis-affected and healthy tendons, and between the torn tendons and tendinosis-affected tissues. To do so, the healthy tissue, tendinosis-affected regions and torn regions of the patellar tendons were manually segmented in B-mode US images obtained from log compression at −13-dB gain, which was used by the physician M.B. while imaging the tendons for diagnosis.

The metrics were measured for US images processed by the three TMOs previously mentioned, as well as conventional log compression at 0 dB (no gain adjustment) and the optimal gain assessed through visual inspection (−17 dB for the simulated phantom and −13 dB for tendon images). To ensure the quality of evaluation, averaged values of the metrics from all relevant images were reported for the *in vivo* scans. One-way analysis of variance and multiple comparison tests were performed for the *in vivo* scans with respect to each metric.

RESULTS

Simulated phantom image

The results of different dynamic range reduction techniques are illustrated in Figure 2, where both Reinhard and Drago TMOs have visibly increased the lesion contrast as well as that of the point scatterers in comparison to the log-compression technique. On the contrary, the image contrast with the Durand TMO appears to be the weakest among the three HDR methods. To confirm the observation, the detailed quantitative evaluations listed in Table 1 were made. The evaluations revealed that all TMOs improved the structural fidelity and image entropy of the LDR

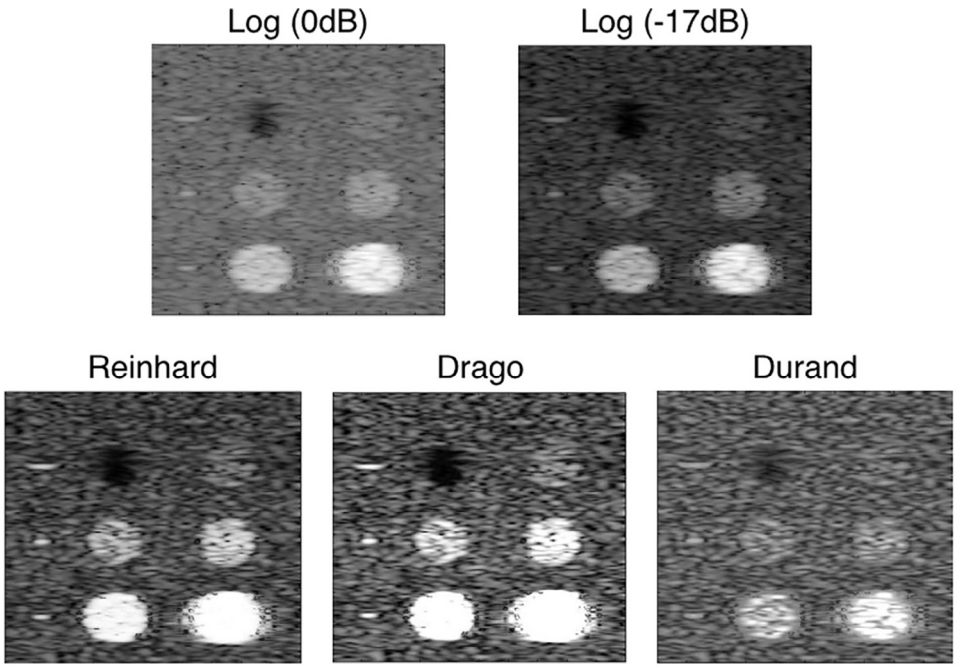

Fig. 2. Different tone mapping operators for the simulated phantom. Tone-mapped results are depicted together with the log-compressed images at 0 and −17 dB.

Table 1. Evaluation of all intensity range reduction techniques on the simulated phantom: SF, image entropy and contrast-to-noise ratios of regions 1–6*

	Log(0 dB)	Log(−17 dB)	Reinhard	Drago	Durand
SF	0.5301	0.6185	0.7850	0.8278	**0.8377**
Entropy	6.2667	6.5394	7.1248	**7.1435**	6.9307
CNR1	3.5430	**3.8950**	3.3496	3.1899	2.0005
CNR2	1.3855	1.4527	**1.5304**	1.5174	0.6740
CNR3	2.8023	2.9464	**3.0962**	3.0700	1.3453
CNR4	3.9351	4.1271	4.5571	**4.6188**	1.8398
CNR5	8.0562	8.7449	**11.4429**	9.3000	3.2145
CNR6	10.9338	11.7368	**13.2426**	9.3740	5.1461

SF = structural fidelity; CNR1–CNR6 = contrast-to-noise ratios of regions 1–6.

* The highest values are in boldface.

images, whereas only Reinhard and Drago TMOs effectively improved the CNRs of the majority of the lesions except the cyst lesion in region 1. The CNRs measured for the Durand TMOs appear to be worse than the rest of the groups. Both qualitatively and quantitatively, Reinhard and Drago TMOs are better choices for reproducing image detail from Hilbert-transformed RF data. Note that lesion 6 (bottom right lesion) appears larger than its real size and also has a blurry boundary because of convergence of the ultrasound wave at high depths (*i.e.,* large point spread function).

In vivo *tendon images*

To qualitatively assess performance of the tone mapping operators, we visually compared the results from different tone mapping operators against the log-compression images at 0 and −13 dB for three patients' patellar tendons. Patient A, as illustrated in Figure 3, had moderate tendinosis without tear, whereas patients B and C, as illustrated in Figures 4 and 5, had moderate tendinosis with small tears in the tendon. Without dynamic range compression, only the bright signals at tissue interfaces (*e.g.,* at bone surfaces) can be displayed (top left of Fig. 4). Different log-compressed images were then generated from the RF signal and visually inspected by M.B. to provide the best contrast for diagnosis. A −13-dB level of log compression (illustrated in Figs. 3–5) was found to provide optimal image quality. The second rows of Figures 3–5 illustrate the results of different TMO techniques. By visual inspection, the Reinhard and Drago TMOs substantially improved overall image contrast and that of the pathologies. Compared with the other two techniques, the Durand TMO better preserved image detail even in the hypoechoic regions of the image, but at a slight cost of the contrast of the tendon pathologies. To confirm the visual evaluation, we measured the structural fidelity, image entropy and CNRs between healthy and tendinosis-affected tissue, as well as between the tear and tendinosis, for all 22 US images, and their averaged values are reported in Table 2. With all 22 sets of scans, one-way analysis of variance and multiple comparison tests revealed that in terms of structural fidelity, all three TMOs outperformed the log-compression techniques ($p < 0.05$), with the Durand TMO achieving the highest score. Reinhard and Drago TMOs ranked first and second in the measurement of image entropy (or image texture) among the group ($p < 0.05$), but the results of the Durand TMO did not statistically differ from those of log compression at −13-dB gain. In terms of CNRs between the healthy and tendinosis-affected tissues, the Durand method is significantly worse than the Reinhard and Drago methods

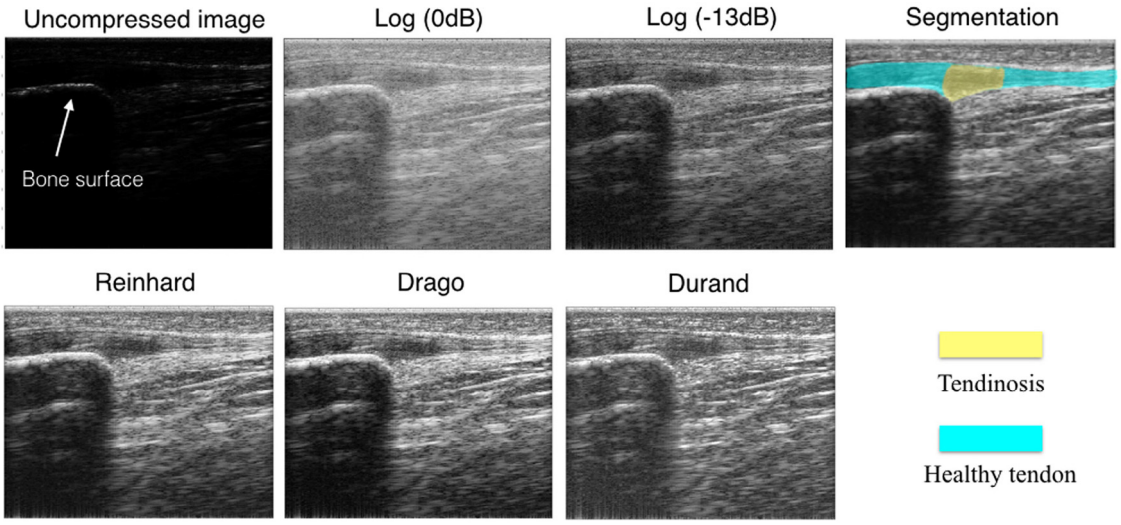

Fig. 3. Different tone mapping operators for patient A. Tone-mapped results are depicted together with the image without intensity compression and log-compressed images at 0 dB and −13 dB. Segmentations of tendon pathologies are shown on the right in the top row.

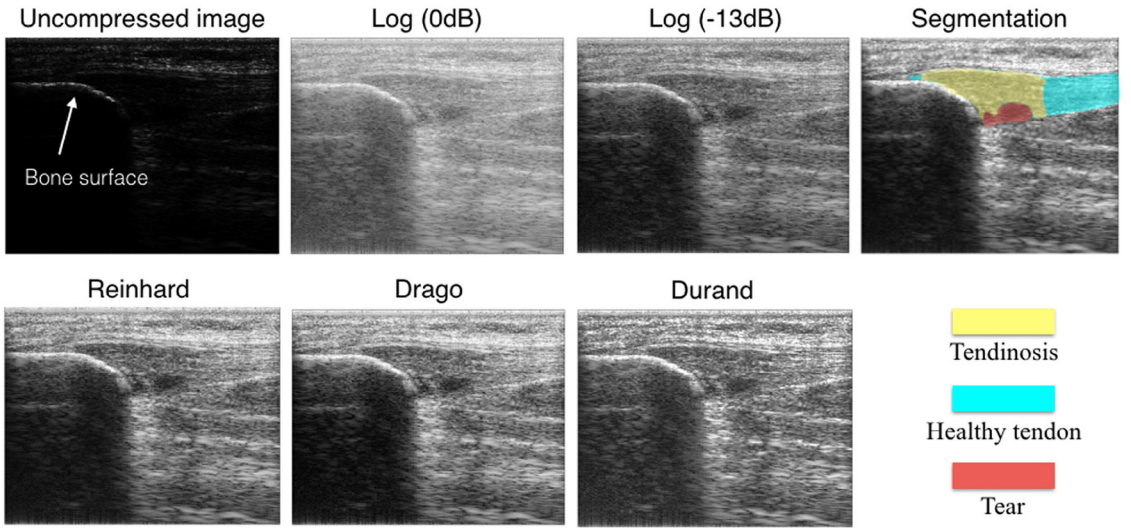

Fig. 4. Different tone mapping operators for patient B. Tone-mapped results are depicted together with the image without intensity compression and log-compressed images at 0 dB and −13 dB. Segmentations of tendon pathologies are shown on the right in the top row.

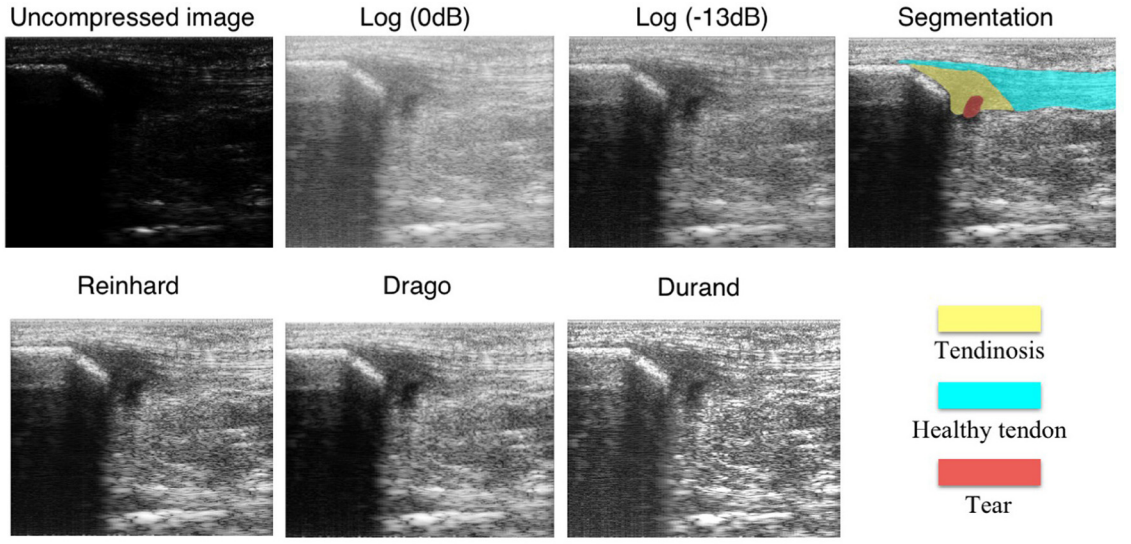

Fig. 5. Different tone mapping operators for patient C. Tone-mapped results are depicted together with the image without intensity compression and log-compressed images at 0 dB and −13 dB. Segmentations of tendon pathologies are shown on the right in the top row.

Table 2. Mean SF, image entropy and contrast-to-noise ratios between healthy and tendinosis tendons (CNR_{ht}) and between torn and tendinosis tendons (CNR_{tt}) for all intensity range reduction techniques*

	Log(0 dB)	Log(−13 dB)	Reinhard	Drago	Durand
SF	0.8926	0.9362	0.9493	0.9582	**0.9681**
Entropy	7.3196	7.5308	7.7013	**7.8179**	7.5320
CNR_{ht}	1.7391	1.7911	**1.8602**	1.8490	1.3411
CNR_{tt}	1.5506	1.6318	1.6396	**1.6440**	1.3173

SF = structural fidelity.
* Highest values are in boldface.

($p < 0.05$), with no difference from the log-compression results at 0 and −13 dB. For the CNR between torn and tendinosis-affected tissues, the Durand method underperformed the Reinhard method, Drago method and log compression at −13 dB ($p < 0.05$), but did not differ from log compression at 0 dB. Although there were no statistical differences among the group when the Durand technique was excluded, the average CNRs of the Reinhard and Drago TMOs are higher than the rest. Based on both qualitative and quantitative evaluations, the Reinhard and Drago techniques were optimal for tendon imaging.

DISCUSSION

We used structural fidelity to evaluate the quality of tone mapping because the commonly used structural similarity (SSIM) index (Wang et al. 2004) can be affected by variations in dynamic ranges (Yeganeh and Wang 2013) and, thus, is mostly used for LDR images. Still rarely used in the medical domain, this metric has also been employed successfully to assess windowing setting for visualization of CT scans (Yeganeh et al. 2012). After review of images at different gains, the best contrasts were selected at gains of −17 and −13 dB for the simulated phantom and tendon images, respectively. By examining the structural fidelity and image entropy for log-compressed images in the range [–50,0] dB with a step size of 1 dB, we found that structural fidelity and image entropy reach maximum values at −17 and −16 dB for the phantom and at −13 and −12 dB for the *in vivo* data. These are consistent with the visual inspection and the choice by the physician.

Previously, there have been other attempts to augment the dynamic range and improve image resolution of B-mode ultrasound signals by using the filtered-delay multiply and sum (F-DMAS) beam-former (Matrone et al. 2015; Ramalli et al. 2017), but these techniques still require signal compression and gain adjustment. In comparison, our technique focuses on mapping of the beam-formed signals to improve visualization. Compared with the rest of the dynamic range reduction methods tested, the Durand TMO provided the best tone mapping quality in terms of structural fidelity measures. This is evidence that it is capable of even preserving speckle patterns in the darker regions from the log-compression images at 0 dB in Figures 3, 4 and 5. However, it failed to improve the image contrast of the lesions in the simulated phantom and tendon pathology. This may largely be due to the fact that, unlike conventional photographs of natural scenes, US images are composed of speckle patterns, which are characteristic with respect to the tissue's biophysical properties and the surrounding environment. Although in some problems, speckles are often regarded as noise and are subject to reduction, the patterns can be helpful in certain scenarios. For example, as the tendons are structures composed of tight collagen fibers, in US images, they appear more texturized in the healthy state. Although the TMO helps to enhance structural detail, the speckles are also emphasized. Thus, both the restricted room for tissue contrast increase due to the limited dynamic range of the display and the enhanced speckles contributed to the low CNR measurements. Yet, by visual inspection of Figures 3–5, the contrast of the tendinosis-affected tissue and small tears is still stronger than that of the log-compressed images at 0 dB.

Although direct analysis of raw RF signals (*e.g.,* image segmentation) can further facilitate tissue classification, the introduced HDR US is not intended to offer such high-level interpretation, but to improve the image display that fully exploits the RF signal in comparison to the conventional method. As a result, unlike direct analysis, its performance is not affected by such factors as the complexity of image content and image characteristics (*e.g.,* noise level). However, qualitative and quantitative analysis can be conducted on the HDR US. Unlike HDR photography, where a series of images taken at different exposures are required, the Hilbert-transformed RF signals from the ultrasound scanner inherently contain the full image detail with extended intensity range. Thus, with access to the RF data, fusing US scans from different gain settings is exempt, and this is especially advantageous in terms of operational and computational efficiency. Therefore, it does not reduce the imaging frame rate. With current computational advancements, it is easy to replace the existing log compression with suitable TMOs to enhance the displayed images, without the constant need to re-adjust image gains. Moreover, additional image processing, such as de-noising (Coupe et al. 2009), can be performed in combination with the tone mapped images to further enhance image quality.

For this study, we focused on *in vivo* tissue, as it is more relevant in the clinic, but the method can also be applied for imaging *ex vivo* tissue for certain studies. However, as *ex vivo* tissue exhibits altered biomechanical and acoustical properties, further evaluation is needed to assess the performance of HDR US in the relevant applications. To illustrate the performance of HDR US, we employed objective metrics that were used to assess the level of image detail and image quality. The limitations of this study lie in the relatively small patient cohort and the lack of correlation between the metrics and clinical assessments. However, the latter requires a larger group of clinicians and more elaborate study protocols. In the future, we intend to conduct more thorough studies on the clinical impacts of the introduced method. More specifically, we will compare HDR US against the conventional log-compression method in terms of qualitative diagnosis and quantitative assessment of lesion size based on a large group of clinicians with various levels of experience and more patient data while using corresponding MRI scans as the reference.

CONCLUSIONS

We proposed to employ HDR processing on US imaging for the first time. Through assessments with objective image quality metrics and visual inspection using a simulated phantom image and *in vivo* images of patellar tendon pathologies, we found that HDR US can enhance anatomic detail and texture, as well as improve the

contrast of tendon pathologies in comparison with conventional US. Of the three popular HDR processing techniques tested, the Reinhard (Reinhard and Devlin 2005) and Drago (Drago et al. 2003) TMOs outperformed the Durand TMO (Durand and Dorsey 2002). The proposed technique does not require manual gain adjustments and, as such, can potentially result in more convenient and less user-dependent sonography. It can potentially help establish B-mode US in longitudinal studies. Besides tendon imaging, the benefits of HDR US may also be easily extended to other applications. With further investigation of its clinical performance using a larger cohort of patients and physicians, the proposed HDR US could have great potential in enhancing the diagnostic value of ultrasonography.

Acknowledgments—This project was partly funded by the Natural Sciences and Engineering Research Council of Canada (NSERC) Discovery Grant RGPIN-2015-04136.

REFERENCES

Achim A, Bezerianos A, Tsakalides P. Novel Bayesian multiscale method for speckle removal in medical ultrasound images. IEEE Trans Med Imaging 2001;20:772–783.

Cincotti G, Loi G, Pappalardo M. Frequency decomposition and compounding of ultrasound medical images with wavelet packets. IEEE Trans Med Imaging 2001;20:764–771.

Coupe P, Hellier P, Kervrann C, Barillot C. Nonlocal means-based speckle filtering for ultrasound images. IEEE Trans Image Process 2009;18:2221–2229.

Drago F, Myszkowski K, Annen T, Chiba N. Adaptive logarithmic mapping for displaying high contrast scenes. Comput Graph Forum 2003;22:419–426.

Durand F, Dorsey J. Fast bilateral filtering for the display of high-dynamic-range images. ACM Trans Graph 2002;21:257–266.

Eilertsen G, Mantiuk RK, Unger J. A comparative review of tone-mapping algorithms for high dynamic range video. Comput Graph Forum 2017;36:565–592.

Jensen JA. Field: A program for simulating ultrasound system. In: 10th NordicBaltic Conference on Biomedical Imaging. Med Biol Eng Comput 1996;4(Suppl 1 Pt 1):351–353.

Lee D, Kim YS, Ra JB. Automatic time gain compensation and dynamic range control in ultrasound imaging systems. Proc SPIE 2006;6147.

Lee Y, Kang J, Yoo Y. Automatic dynamic range adjustment for ultrasound B-mode imaging. Ultrasonics 2015;56:435–443.

Matrone G, Savoia AS, Caliano G, Magenes G. The delay multiply and sum beamforming algorithm in ultrasound B-mode medical imaging. IEEE Trans Med Imaging 2015;34:940–949.

Moshavegh R, Hemmsen MC, Martins B, Hansen KL, Ewertsen C, Brandt AH, Bechsgaard T, Nielsen MB, Jensen JA. Advanced automated gain adjustments for in-vivo ultrasound imaging. Proc IEEE Int Ultrason Symp 2015;1–4. doi:10.1109/ULTSYM.2015.0298.

Perperidis A. Postprocessing approaches for the improvement of cardiac ultrasound B-mode images: A review. IEEE Trans Ultrason Ferroelectr Freq Control 2016;63:470–485.

Peters SA, Bots ML, Lind L, Groenewegen KA, de Korte C, den Ruijter HM. Meteor Study Group. The impact of variability in ultrasound settings on the measured echolucency of the carotid intima–media. J Hypertens 2013;31:1861–1867.

Potter K, Reed CJ, Green DJ, Hankey GJ, Arnolda LF. Ultrasound settings significantly alter arterial lumen and wall thickness measurements. Cardiovasc Ultrasound 2008;6:6.

Ramalli A, Dallai A, Bassi L, Scaringella M, Boni E, Hine GE, Matrone G, Savoia AS, Tortoli P. High dynamic range ultrasound imaging with real-time filtered-delay multiply and sum beamforming. Proc IEEE Int Ultraon Symp 2017. doi:10.1109/ULTSYM.2017.8091860.

Reinhard E, Devlin K. Dynamic range reduction inspired by photoreceptor physiology. IEEE Trans Vis Comput Graph 2005;11:13–24.

Shapiro RS, Wagreich J, Parsons RB, Stancato-Pasik A, Yeh HC, Lao R. Tissue harmonic imaging sonography: Evaluation of image quality compared with conventional sonography. AJR Am J Roentgenol 1998;171:1203–1206.

Tomasi C, Manduchi R. Bilateral filtering for gray and color images. New York: IEEE; 1998. p. 839–846. ICCV '98—Proceedings of the Sixth International Conference on Computer Vision.

Wang Z, Bovik AC, Sheikh HR, Simoncelli EP. Image quality assessment: From error visibility to structural similarity. IEEE Trans Image Process 2004;13:600–612.

Yeganeh H, Wang Z. Objective quality assessment of tone-mapped images. IEEE Trans Image Process 2013;22:657–667.

Yeganeh H, Wang Z, Vrscay ER. Adaptive windowing for optimal visualization of medical images based on a structural fidelity measure. Lect Notes Comput Sci 2012;7325:321–330.